

The formation of microsplits and damage rafts in proton-bombarded GaAs

J. H. NEETHLING, H. C. SNYMAN

Department of Physics, University of Port Elizabeth, PO Box 1600, Port Elizabeth 6000, Republic of South Africa

The technique of cross-sectional transmission electron microscopy has been used to study the nature and formation of damage rafts, which act as dislocation sources, in proton-bombarded (5×10^{15} , 10^{16} and 10^{17} $\text{H}^+ \text{cm}^{-2}$) and annealed GaAs. The results show that the rafts consist of a planar array of voids lying on the $\{110\}$ cleavage planes of GaAs. The dislocations generated at these rafts are glissile, of the $(a/2) \langle 110 \rangle$ type, and glide on the $\{111\}$ planes intersecting the rafts. Models are presented to show that these damage rafts originated at microsplits on the $\{110\}$ cleavage planes of GaAs following the cracking open of small hydrogen-filled platelets on $\{110\}$ planes when the internal gas pressure exceeds that which is necessary for crack propagation. From the analysis of the results an average diffusion length of $\sim 1 \mu\text{m}$ was estimated for vacancies in proton-bombarded GaAs at $\sim 900^\circ\text{C}$.

1. Introduction

Proton bombardment of crystalline gallium arsenide has now become a standard technique in the fabrication of various optoelectronic devices, such as low-loss optical waveguides [1], isolated p-n junction diodes and semiconductor lasers [2]. During proton bombardment lattice defects are introduced which, although required to produce a high resistivity in the implanted layer, can have detrimental effects on device performance. It is the realization of this latter fact that has motivated a systematic transmission electron microscopy (TEM) investigation of the lattice defects in GaAs subjected to doses of 10^{15} to 10^{17} $\text{H}^+ \text{cm}^{-2}$. The preliminary findings of this investigation were published in a number of papers [3-5].

In a recent paper [6] we have shown that the precipitated damage in low-dose (5×10^{15} $\text{H}^+ \text{cm}^{-2}$) proton-bombarded and annealed (temperatures of between 500 and 800°C) GaAs consists of small hydrogen platelets (i.e. hydrogen-filled vacancy loops) on the $\{110\}$ planes of GaAs. This finding is in contrast to the earlier identification [3, 4] of these loop-like defects as Frank vacancy loops on the $\{111\}$ planes.

For higher proton doses and temperatures of anneal, however, additional defect components in the form of damage rafts, dislocations and voids were observed in the damage layer [5, 7]. It is the purpose of this paper to show that these damage rafts originate at microsplits on the $\{110\}$ cleavage planes of GaAs following the cracking open of small hydrogen-filled platelets when the internal gas pressure exceeds that which is necessary for crack propagation. Models are also presented to explain the observed generation of glissile dislocations at the rafts.

Finally the close resemblance between the damage rafts (and dislocations generated at the rafts) and the

dark-line defects found in degraded $\text{Ga}_{1-x}\text{Al}_x\text{As}$ laser devices is discussed.

2. Experimental procedure

The n-type silicon-doped (10^{18} carriers cm^{-3}) GaAs samples were bombarded at 7° off the $[001]$ axis with 300 keV protons to total doses of 5×10^{15} , 10^{16} and 10^{17} $\text{H}^+ \text{cm}^{-2}$ using a beam current of $0.1 \mu\text{A}$. All implantations were carried out at room temperature in an HVEE 350 keV ion implanter using H_2S gas as the source material. The crystals, $300 \mu\text{m}$ in thickness, were subsequently laser-scribed along the $\langle 110 \rangle$ direction on the back and then cleaved in rodlike samples 4 mm by 1 mm. After slicing, capless annealing experiments were carried out in which the samples were heated (implanted surface down) for 15 min at various temperatures between 300 and 900°C in an argon atmosphere. The samples were then quenched to room temperature by dropping them into water. For transmission electron microscopy the samples were thinned in cross-section, first mechanical-chemically, and finally by argon ion-milling.

3. Experimental results and analysis

3.1. The nature of the damage rafts

Examination of the damaged layer about the average projected range in low-dose proton-bombarded GaAs annealed at elevated temperatures showed that, in contrast to the lower-temperature-annealed samples [6], the damage precipitation was heterogeneous consisting not only of platelets but also containing damage rafts, voids and dislocations. The critical dose and temperature required for raft formation were found to be 5×10^{15} $\text{H}^+ \text{cm}^{-2}$ annealed at 800°C , or 10^{16} $\text{H}^+ \text{cm}^{-2}$ annealed at 500°C for 15 min. That these damage rafts [4] are associated with the damage layer (i.e. the stopping zone of the protons) is very

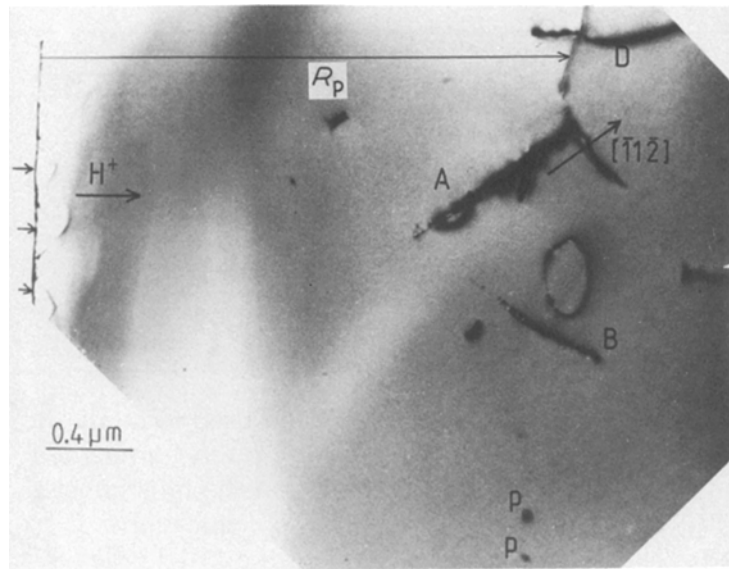


Figure 1 The defect structure in proton-bombarded ($10^{16} \text{H}^+ \text{cm}^{-2}$ at 300 keV) GaAs annealed at 800°C for 15 min. Damage rafts are indicated by A and B, dislocations by D and platelets by P.

clearly illustrated in Fig. 1, which shows the damage layer in a GaAs sample bombarded to a dose of $10^{16} \text{H}^+ \text{cm}^{-2}$ at 300 keV and annealed at 800°C . The Lindhard, Schanff and Schiott (LSS) projected range [8] for the protons is indicated by R_p , while the rafts, dislocations and platelets are indicated by A, D and P, respectively. The thermal etch pits (seen in cross-section), indicated by the arrows at the surface in Fig. 1, results from the out-diffusion of arsenic because a capless annealing procedure in an argon atmosphere was used. These etch pits, having a maximum depth of $\sim 0.1 \mu\text{m}$, are not expected to influence the radiation damage which is at the much greater depth of $\sim 2.5 \mu\text{m}$ for protons with an energy of 300 keV. The black strip covering the etch pits is due to the glue that was used in the bonding of the cross-sectional strips.

In Fig. 2 the damage layer in a proton-bombarded sample is shown in two sections. The damage rafts are indicated by A, B and C and some of the platelets by P. The dislocations indicated by D were probably generated at the rafts and will be discussed in Section 3.4. A detailed analysis of the geometry of the rafts, by tilting them into edge-on configurations in the TEM, revealed that they consist of planar arrays of voids on the $\{110\}$ planes of GaAs and are elongated along the $\langle 110 \rangle$ directions. The rafts indicated by A, B and C in Fig. 2 lie on the $(10\bar{1})$, (101) and (101) planes, respectively. Rafts B and C are also elongated along the $[10\bar{1}]$ direction and Raft A along a direction close to the $[101]$. A (110) projection of the images of Rafts A, B and C will therefore lie along the $[\bar{1}1\bar{2}]$, $[1\bar{1}\bar{2}]$ and $[1\bar{1}\bar{2}]$ directions, respectively, as indicated in Fig. 2.

It is suggested that the rafts originate at microsplits which form on the $\{110\}$ cleavage planes [9] to relieve the stresses due to the hydrogen gas from the proton bombardment. A microsplit forms a free surface inside the crystal and thus act as a sink for getting the surrounding vacancies [10, 11]. If a sufficient number of vacancies are absorbed at the free surfaces of the microsplit, voids will start to form in the plane of the split and relaxation of internal stress in the

crystal may lead to closure of the microsplits. When this occurs, but the two surfaces do not align crystallographically perfectly, dislocations will be introduced to relieve the lateral mismatch of the two displaced surfaces. In the following sections this assumption that mismatch of the two $\{110\}$ surfaces introduces dislocations is verified experimentally.

A magnified image of the raft indicated by C in Fig. 2 is shown in Figs 3a and b under dynamical and kinematical diffraction conditions, respectively. In Fig. 3a the voids are obscured by the strain contrast generated at the raft. In Fig. 3b the planar array of faceted voids is clearly visible when viewed almost edge-on under kinematical diffraction conditions. In Fig. 3c the raft image is changed from that observed for the edge-on configuration (Figs 3a and b) to a more planar view by tilting 40° clockwise about $[1\bar{1}0]$. The two-dimensional character of the rafts is clearly demonstrated by this micrograph. In Fig. 3 the dislocations in the (101) split plane, which are a result of the imperfect closure of the split, are also visible.

The image characteristics of the voids observed in the rafts were studied by viewing them under dynamical and kinematical diffraction conditions and also in underfocused and overfocused conditions. In Fig. 4 a planar array of small voids associated with a damage raft is shown. Small voids are much more visible when the image is slightly out of focus and viewed under kinematical diffraction conditions. In an underfocus condition the void image is bright relative to the background and the image has a dark rim. In an overfocus condition the void is a dark image with a faint bright rim [12]. All these image characteristics are displayed by the voids shown in Figs 4a and b. When small voids are viewed under dynamical diffraction conditions with the Bragg deviation parameter $w \sim 0$, the image contrast of the voids depends on the foil thickness and the depth of the void in the foil. Computed intensity profiles for small voids ($r = 2 \text{ nm}$) in silicon, calculated under dynamical diffraction conditions with $w \sim 0$, indicated that these voids can exhibit black-white or black dot images depending on the foil thickness and depth of the void in the foil [13].

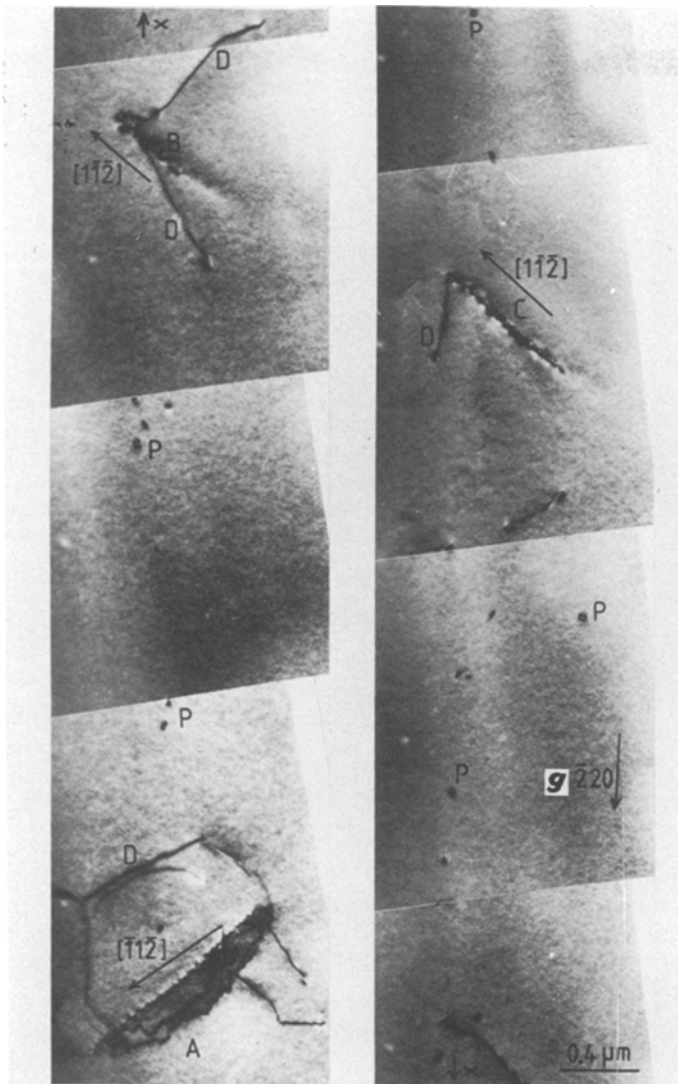


Figure 2 Cross-sectional view of the damaged layer parallel to the implanted (001) surface, shown in two sections for clarity. Areas corresponding to the same point are indicated by \times . Rafts A, B and C lie on the (10 $\bar{1}$), (101) and (101) planes, respectively. The dose is 10^{16} H $^+$ cm $^{-2}$ at 300 keV and the specimen was annealed at 800°C for 15 min. The electron beam is close to the $[\bar{1}\bar{1}0]$ direction.

In Fig. 4c an example of the black dot void images is shown when the voids in Figs 4a and b are viewed under dynamical diffraction conditions with $w \sim 0$ and in focus. These results verify that the black dot images which are sometimes observed in rafts under certain imaging conditions (see Fig. 5a) are indeed voids and not holes.

In Fig. 5a an example of a raft (A) on the (110) plane is shown. It can be seen that the raft is elongated along the $[\bar{1}\bar{1}0]$ direction. It will be shown in Section 3.2 that the theoretical fracture stress is lower for cracking in the $[\bar{1}\bar{1}0]$ than in the perpendicular [001] direction; thus the crack (split) will spread easier in the $[\bar{1}\bar{1}0]$ than the [001] direction. This anisotropic

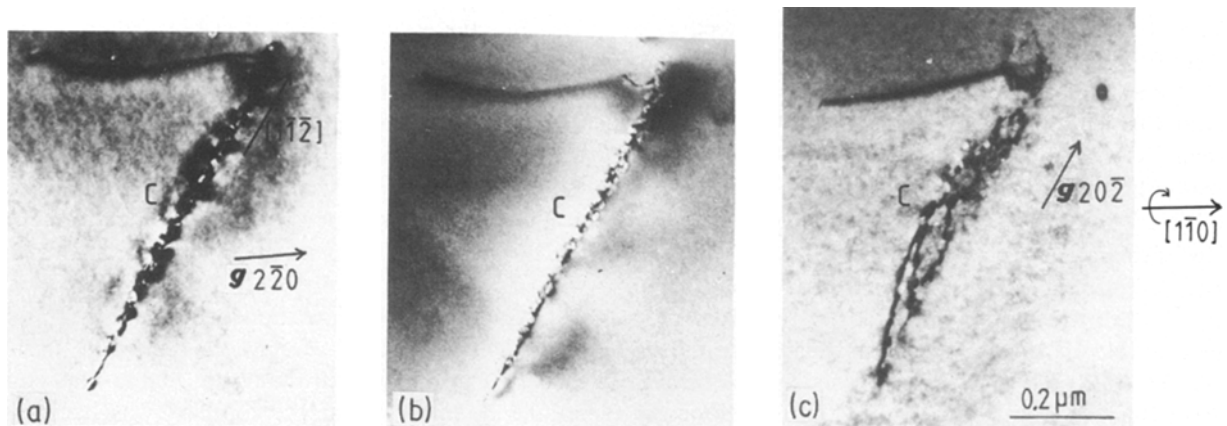


Figure 3 Magnified image of raft on (101) plane (indicated by C in Fig. 2) shown under (a) dynamical and (b) kinematical diffraction conditions. In (a) the voids are obscured by the strain contrast of the raft. In (c) the raft image is changed from the edge-on configuration in (a) and (b) to an inclined configuration by a 40° clockwise tilt about $[\bar{1}\bar{1}0]$. The two-dimensional character of the rafts is clearly illustrated by these micrographs, and in (c) dislocations in the raft plane are also visible. The beam axis in (a) and (b) is close to $[\bar{1}\bar{1}0]$ and in (c) it is close to the $[\bar{1}\bar{1}\bar{1}]$ direction.

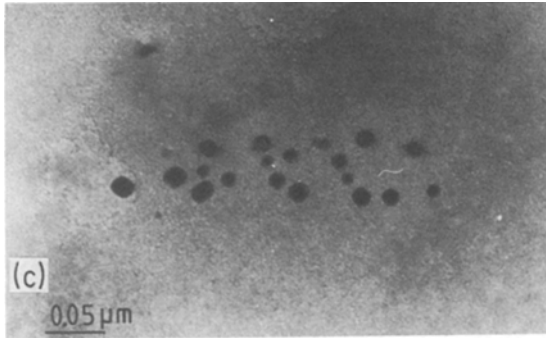
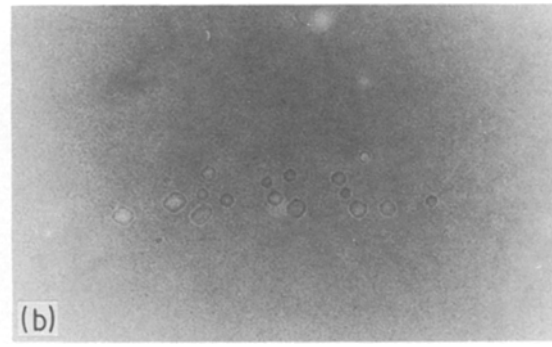
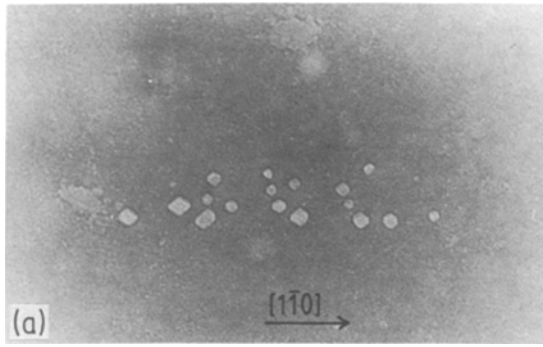


Figure 4 Small voids observed in proton-bombarded ($10^{16} \text{ H}^+ \text{ cm}^{-2}$ at 300 keV) and annealed (800° C for 15 min) GaAs. The viewing conditions are the following: (a) kinematical diffraction conditions, underfocussed, (b) kinematical diffraction conditions, overfocussed, (c) dynamical diffraction conditions, in-focus with $w \sim 0$ and $g = 2\bar{2}0$. The beam axis is close to the $[\bar{1}\bar{1}0]$ direction in all cases.

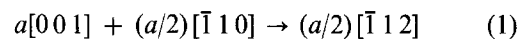
property explains the observed elongation of the rafts along the $\langle 110 \rangle$ directions.

The presence of the voids and dislocations in the raft plane is consistent with the identification of a damage raft as a microsplit which has closed, but healed imperfectly. By means of tilting experiments, it was established that the half-loop E (Fig. 5a), which is generated at the raft, spreads out on the (111) slip plane which intersects the raft on the (110) plane. The generation of similar types of dislocation at the rafts is discussed in Section 3.4. In Fig. 5b the dislocations in the (110) plane of the split are more clearly visible under the $g = 20\bar{2}$ diffraction condition. The zigzag nature of these dislocations is typical of those introduced when a crack (split) on the $\{110\}$ planes of the zincblende structure heals imperfectly as theoretically predicted by Allen [14].

The directions of the Burgers vectors of the dislocations in the raft were determined from the usual $g \cdot b = 0$ invisibility criterion. It will be shown that some of the dislocations in the raft, introduced as a result of the mismatch of the two (110) surfaces, could possibly have unit Burgers vectors of the type $\pm a[001]$ or $\pm (a/2)[\bar{1}10]$ in the plane of the split. The possibility that such types of edge dislocation can form in GaAs has been suggested by Hutchinson and Dobson [15, 16]. From Figs. 5c and d, where a planar view of the rafts is obtained by tilting to a $[\bar{1}\bar{1}0]$ beam axis, it is clear that the dislocation segments parallel to the $[\bar{1}10]$ direction and indicated by the arrows (1) are invisible in the $g = 2\bar{2}0$ diffraction condition (Fig. 5c) and could thus be interpreted as dislocations with a Burgers vector of the type $\pm a[001]$. Similarly the dislocation segments in Fig. 5c indicated by (2) are invisible under $g = 00\bar{4}$ and could thus be of the type $\pm (a/2)[\bar{1}10]$. Both these dislocations are not contained within a close-packed plane of the face-centred cubic structure, and thus since they are sessile a jagged

configuration of dislocation networks could be expected. Edge dislocations with a Burgers vector of the type $b = (a/2)\langle 110 \rangle$ have been observed by Comer [17] in microcracks on $\{110\}$ cleavage planes in InP.

A very interesting part of the raft, which is more clearly visible in a steeply inclined configuration in Fig. 5e, is that indicated by the arrows (3) in Figs 5c, d and e. These dislocations appear very similar to the dislocation networks observed by Hutchinson and Dobson [15] in degraded GaAs lasers. However, inside/outside contrast experiments performed on the raft, and in particular the part visible in Fig. 5e, revealed that the raft consists of line dislocations on the (110) planes, in contrast to the results of Hutchinson and Dobson who found that their dislocation networks were dislocation dipoles of extrinsic nature. The segments of the dislocation network parallel to the $[\bar{1}10]$ direction, and indicated by the arrows (3), were found to be visible under all the diffraction conditions used (i.e. $g = 2\bar{2}0, 00\bar{4}, \bar{2}20, 0\bar{2}2$ and $20\bar{2}$). The most likely Burgers vector for this network is that produced by a displacement in the $\pm [\bar{1}12]$ or $\pm [1\bar{1}2]$ directions. The proposed Burgers vector for this displacement is given by the reaction



The Burgers vector $b = (a/2)[\bar{1}12]$, which satisfies the condition $g \cdot b \neq 0$ for the different diffraction vectors used, is a fundamental translation vector and thus a possibility for a Burgers vector. Although this Burgers vector is not usually associated with the GaAs structure, such a displacement (as given by the reaction in Equation 1) is possible when reconstruction of the two (110) surfaces of the split occurs. The only way of testing the validity of the identification of the dislocation given by Equation 1 is by imaging under $g = \langle 111 \rangle$ reflection conditions perpendicular to the $\langle 112 \rangle$ directions in the (110) plane. This could not be done as the defect complex was lost when *in situ* heating experiments ($\sim 580^\circ \text{ C}$ for 10 min) were carried out to study the dynamics of the defects on heating. However, the important observation that the dislocation half-loop E glides out fairly easily on the (111) plane, while the jagged network retains its

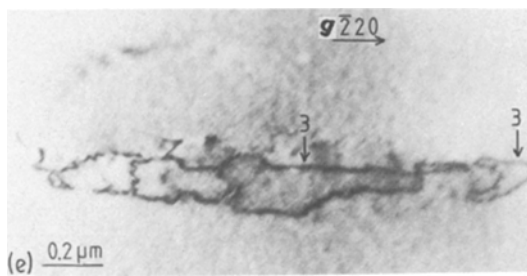
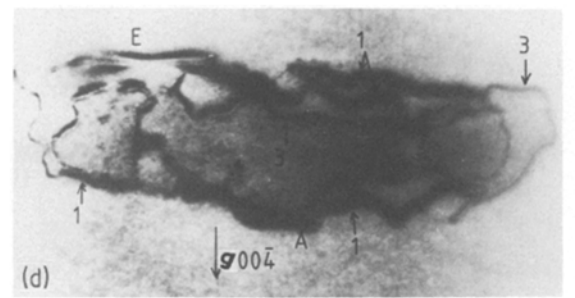
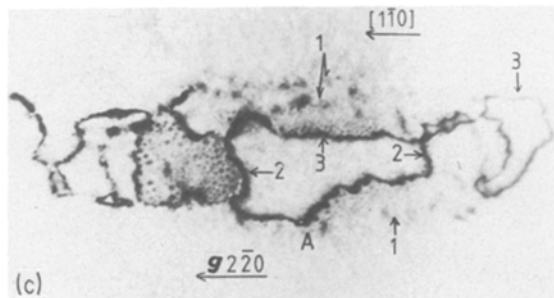
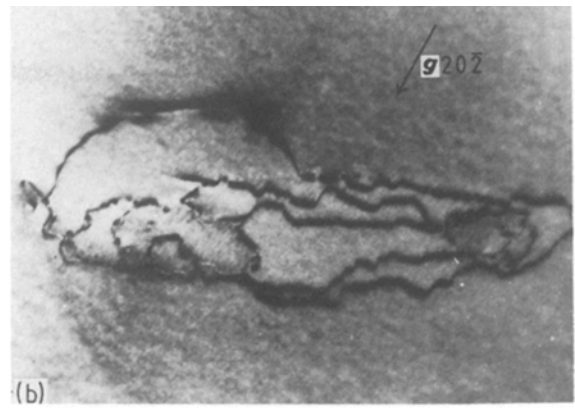
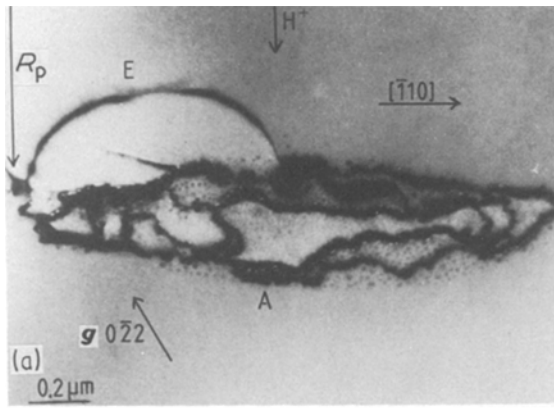


Figure 5 A planar view of a damage raft (A) on a (110) plane of a GaAs sample bombarded with 300 keV protons to a dose of $10^{16} \text{H}^+ \text{cm}^{-2}$ and annealed for 15 min at 800°C . The half-loop E is generated at the raft and spreads out on the (111) slip plane. The projected range of the protons is indicated by R_p . The beam axis in (a) and (b) is close to $[\bar{1}\bar{1}\bar{1}]$, in (c) and (d) close to the $[\bar{1}\bar{1}0]$ and in (e) close to $[\bar{1}\bar{1}2]$. All the micrographs were recorded with the Bragg deviation vector, s , slightly larger than zero.

configuration, was made prior to disintegration of the sample. This observation is consistent with the identification of the dislocations in the (110) plane of the raft as sessile dislocations which cannot glide.

The structure of the damage layer of the heavily bombarded ($10^{17} \text{H}^+ \text{cm}^{-2}$) GaAs samples differed strikingly from that of the low-dose samples. Radiation damage was detectable in these samples without annealing [3, 4]. An example of the precipitated damage in a sample bombarded with 300 keV protons at $10^{17} \text{H}^+ \text{cm}^{-2}$ and annealed at 600°C is shown in Fig. 6a. The LSS projected range [8] for 300 keV protons is indicated by R_p . Examination of the damage layer (Fig. 6a) revealed that it consists of hydrogen platelets (visible as black dots in the surface layer) indicated by P and a high density of crystal effects (visible as a dark diffuse band on the micrograph) which make the sample almost opaque to 100 kV electrons. The damage rafts in these samples that could be distinguished from the dark band of defects were visible in the form of rods along the $\langle 112 \rangle$ directions. In Fig. 6a an example of a raft (A) lying on the (10 $\bar{1}$) plane is shown. The (110) projected image of the raft is seen to lie along the $[\bar{1}\bar{1}2]$ direction. In Fig. 6b the defect structure in Fig. 6a is shown at a higher magnification. Similar features are observed in a sample bombarded with $5 \times 10^{16} \text{H}^+ \text{cm}^{-2}$ and annealed at 700°C as indicated

by E and F in Fig. 6c. In this case the images of the rafts, which most likely lie on the (10 $\bar{1}$) planes, are projected along the $[\bar{1}\bar{1}2]$ direction. In Fig. 6d, voids present in the rafts and in the damaged layer of a proton-bombarded ($10^{17} \text{H}^+ \text{cm}^{-2}$ and annealed at 600°C) sample are clearly visible. The two rafts, indicated by G and H, are projected along the $[\bar{1}\bar{1}2]$ direction. In the raft indicated by H, the coalescence of voids in the plane of the raft (or microsplit) has resulted in the formation of a planar cavity which most likely lies on the (01 $\bar{1}$) plane and is elongated in the [011] direction. A significant feature of this micrograph (Fig. 6d) is that the damage rafts in the heavily bombarded samples consist of planar arrays of voids similar to those found in the lower-dose samples as discussed in the previous paragraphs.

3.2. Theoretical fracture stress of GaAs

In the present case an extension of the Griffiths fracture analysis was used to determine the order of magnitude of the pressure inside a platelet required for crack propagation. According to Messmer and Bilello [18] the stress required to produce brittle fracture on the $\{110\}$ planes under plane strain is given by

$$\sigma = [2E_{110}\gamma_c/(1 - \nu^2)\pi c]^{1/2} \quad (2)$$

where σ = stress applied normal to the $\{110\}$ planes, E_{110} = Young's modulus in the $\langle 110 \rangle$ direction, γ_c = cleavage surface energy of the $\{110\}$ planes,

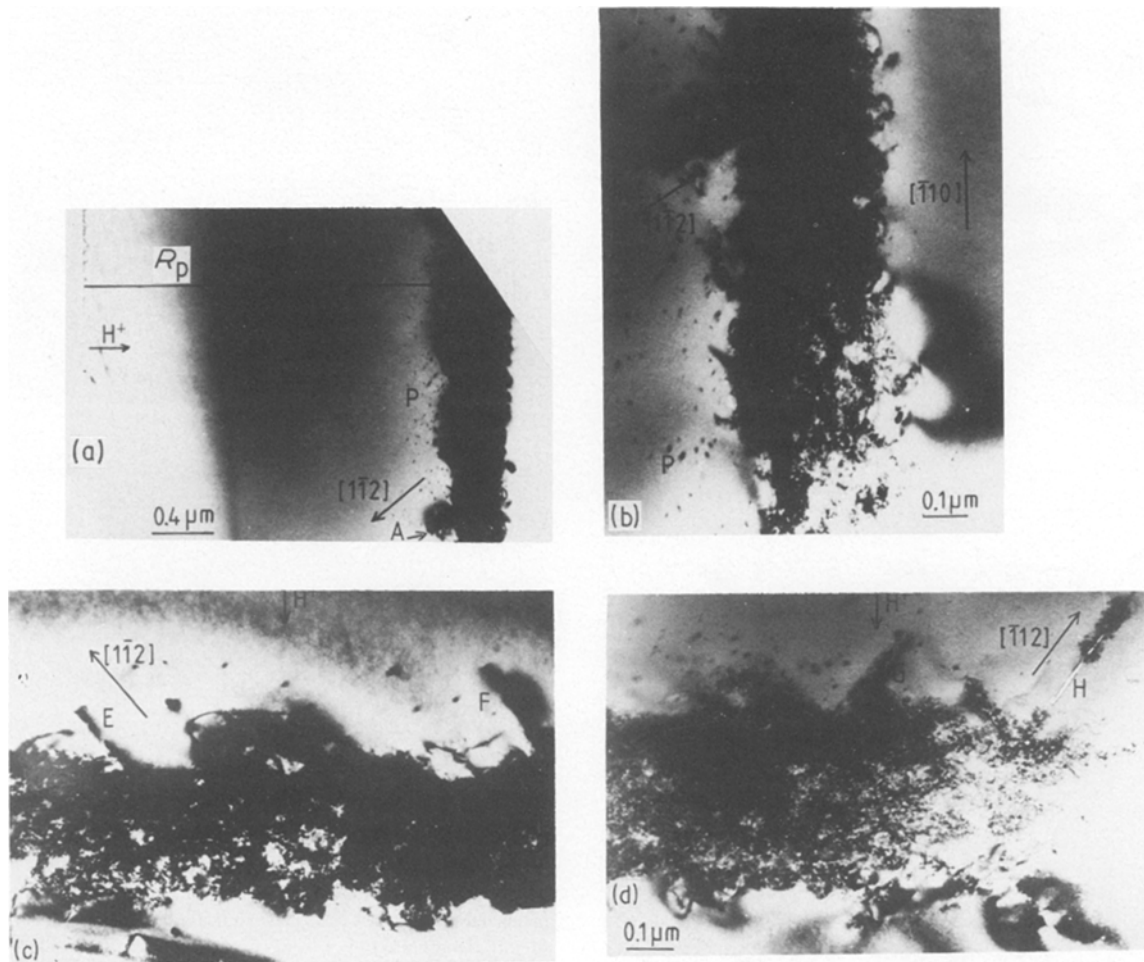


Figure 6 Defect structure in GaAs bombarded with 300 keV protons. (a) The damage raft is indicated by A and the hydrogen platelets by P (dose $10^{17} \text{ H}^+ \text{ cm}^{-2}$, annealed at 600° C for 15 min). (b) Micrograph showing the defect structure in (a) at a higher magnification. (c) The damage rafts are indicated by E and F (dose $5 \times 10^{16} \text{ H}^+ \text{ cm}^{-2}$, annealed at 700° C for 15 min). (d) The damage rafts are indicated by G and H (dose $10^{17} \text{ H}^+ \text{ cm}^{-2}$, annealed at 600° C for 15 min). The electron beam is close to the $[\bar{1}\bar{1}0]$ direction in all the micrographs.

ν = Poisson's ratio and c = half-width of an elliptical cavity.

If the shape of the bowed-out $\{110\}$ planes of a pressurized hydrogen platelet is, as a first approximation, considered to be analogous to an elliptical cavity (with c = platelet radius) on a $\{110\}$ plane stressed in plane strain, then Equation 2 may be applied to obtain

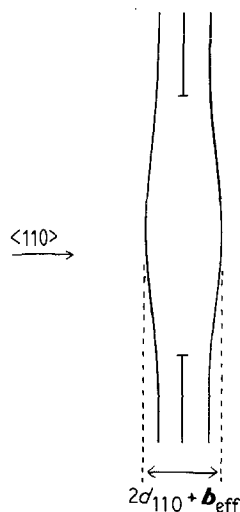


Figure 7 Schematic representation of the distortion of the $\{110\}$ lattice planes produced by a hydrogen platelet.

the gas pressure in a platelet required to propagate a crack along the $\{110\}$ planes.

In recent papers [6, 19] we have suggested that the lattice distortion caused by a hydrogen platelet will most likely be of the form shown in Fig. 7. A platelet can thus be characterized by an effective Burgers vector (b_{eff}) [6, 7, 19] equal to the total outward displacement of the two $\{110\}$ lattice planes relative to one another at the centre of the platelet. The determination of the effective Burgers vectors of the platelets and the calculation of the gas pressures inside the platelets were published elsewhere [7, 19, 20].

In order to obtain the dependence of the fracture stress upon crystal temperature, σ was calculated for different temperatures. Since data on the variation of γ_c with temperature was not available, only the temperature dependence of E and ν could be used to determine the variation of σ with temperature. E and ν were calculated using the expressions given by Brantley [21] and the elastic stiffness constants of Cottam and Saunders [22] and Burenkov *et al.* [23]. The results of the calculations are listed in Table I where l is a unit vector in the direction of the applied stress and m a unit vector along the direction of the resultant strain perpendicular to l .

For the purpose of illustration, we calculate the fracture stress for a platelet radius of 12.4 nm (i.e.

TABLE I Young's modulus E and Poisson's ratio ν for GaAs for directions $l = [011]$ and $m = [0\bar{1}1]$ for the temperature range 298 to 1073 K

Temperature (K)	E (10^{11} N m^{-2})	ν
298	1.207	0.021
873	1.127	0.015
1073	1.103	0.014

$c = 12.4 \text{ nm}$). Taking $\gamma_c = 0.86 \text{ J m}^{-2}$ [18] and E_{110} and ν as listed in Table I, the fracture stress was calculated as a function of temperature and the results are tabulated in Table II. It is interesting to notice, if γ_c is assumed to be constant, that the fracture stress does not change significantly with temperature in the range 298 to 1073 K.

Because of the elastic anisotropy of GaAs it was necessary to take into account the variation of σ with crystallographic directions in the $\{110\}$ planes. E and ν were again calculated using the expressions given by Brantley [21]. Young's modulus E for the $\langle 011 \rangle$ directions which lie in the $\{100\}$ planes was calculated to be $1.207 \times 10^{11} \text{ N m}^{-2}$ at 298 K. The values obtained for Poisson's ratio for directions lying in the $\{011\}$ planes are tabulated in Table III, where l and m are the same as defined before. Using Equation 2 and taking $\gamma_c = 0.86 \text{ J m}^{-2}$, $E_{110} = 1.207 \times 10^{11} \text{ N m}^{-2}$ and ν as listed in Table III, the fracture stress for a hydrogen platelet with radius 12.4 nm (i.e. $c = 12.4 \text{ nm}$) was calculated for various directions in a (011) plane, and the results are tabulated in Table IV.

It is clear from the results listed in Table IV that the fracture stress increased by approximately 10% with crystallographic direction going from the $[0\bar{1}1]$ to the $[100]$ direction in the (011) plane. A physical explanation for this phenomenon can be given if the GaAs crystal structure is viewed along the $[\bar{1}00]$ and perpendicular $[0\bar{1}1]$ directions as shown in Fig. 8. For a given longitudinal stress applied in the direction $l = [011]$, one would expect a smaller transverse strain along the orthogonal direction $m = [01\bar{1}]$ than along the direction $m = [\bar{1}00]$. This effect arises due to the difference in atomic configuration in the GaAs structure when viewed along the $[\bar{1}00]$ and $[0\bar{1}1]$ directions as shown in Figs 8a and b. Due to the straight nature of the atomic bonds along the $[011]$ direction when viewed along the $[\bar{1}00]$ direction (see Fig. 8a), the atoms are held more rigidly and displacement in the $[01\bar{1}]$ direction, due to the bond-angle changes, is not possible. In the $[\bar{1}00]$ direction, since the atomic bonds run in a zigzag fashion (see Fig. 8b), a larger contraction is possible as the covalent bond angles increase. The smaller value of ν in the $[01\bar{1}]$ than in the $[\bar{1}00]$ direction is thus understood in terms of the difference in covalent bond angles in these two

TABLE II Theoretical fracture stress σ in the $[1\bar{1}0]$ direction as a function of temperature for platelet (with radius = 12.4 nm) on a (110) plane of GaAs

Temperature (K)	σ (10^9 Pa)
298	2.31
873	2.23
1073	2.21

directions. From Equation 2 it follows that the fracture stress σ is proportional to $(1 - \nu^2)^{-1/2}$ and therefore σ will increase with increasing ν for a given E . This argument explains the variation of fracture stress with crystallographic directions in $\{110\}$ planes as can be seen from the results listed in Table IV. These results will be used to explain the elongated shape of the damage rafts in Section 3.4.

Finally, in order to show that the coalescence of overpressurized platelets can result in microsplit formation, it was necessary to calculate the fracture stress as a function of platelet radius. Using Equation 2 and taking $E_{110} = 1.207 \times 10^{11} \text{ N m}^{-2}$, $\gamma_c = 0.86 \text{ J m}^{-2}$ and $\nu = 0.021$, the fracture stress in the $[0\bar{1}1]$ direction for a platelet on a (011) plane was calculated as a function of the platelet radius and the results are tabulated in Table V. The variation of the theoretical fracture stress with platelet radius is graphically illustrated in Fig. 9. The significance of the results listed in Table V is discussed in the next section.

3.3. Microsplit formation

The pressure necessary for crack propagation (i.e. the theoretical fracture stress) decreases with platelet radius as shown in Fig. 9 and Table V. For comparison the experimentally determined pressures inside the platelets as a function of platelet radius are also plotted in Fig. 9. The temperature was chosen as 800°C since microsplits were first observed at this temperature in samples subjected to a proton dose of $5 \times 10^{15} \text{ H}^+ \text{ cm}^{-2}$. The pressures were calculated using van der Waal's equation [7, 19].

In the present study it was assumed, for the purpose of the calculations and discussions, that the platelets were formed by the removal of a double $\{110\}$ layer of GaAs atoms [6, 7, 19]. The pressures obtained for these platelets are indicated by the words "one double $\{110\}$ layer" in Fig. 9. It is possible, however, that more $\{110\}$ layers can be removed during the growth process of the platelets. This increase in platelet volume will cause an increase in the calculated pressures; however, it will not change the measured value of b_{eff} , since the removal of two or three additional double $\{110\}$ layers will not affect the strain contrast image of the platelet within the limit of resolution of the electron microscope. The possibility that a platelet can consist of more than one atomic

TABLE III Calculated values for Poisson's ratio ν for GaAs at 298 K

Crystal plane and directions	(100) $l = [011]$ $m = [0\bar{1}1]$	(21 $\bar{1}$) $l = [011]$ $m = [1\bar{1}1]$	(23 $\bar{3}$) $l = [011]$ $m = [3\bar{1}1]$	(0 $\bar{1}1$) $l = [011]$ $m = [100]$
ν	0.021	0.162	0.366	0.443

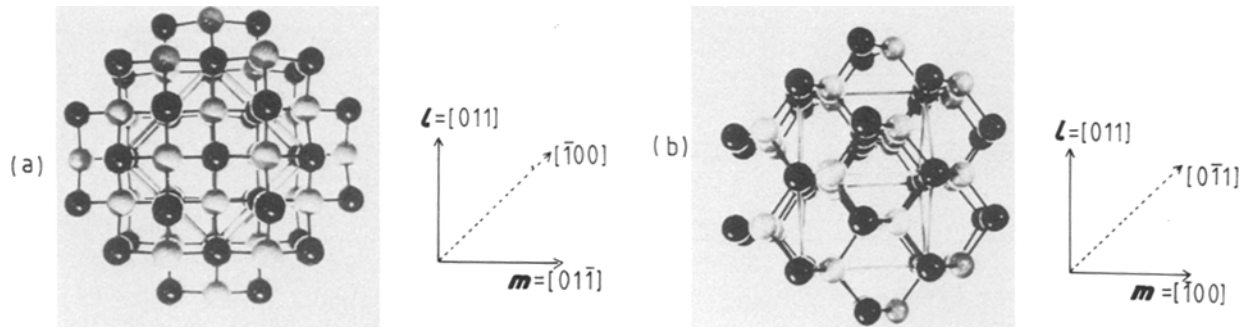


Figure 8 Schematic representation of the crystal structure of GaAs viewed along (a) the $[\bar{1}00]$ direction and (b) the $[0\bar{1}1]$ direction.

layer has been suggested by Evans *et al.* [24] in the case of helium platelets in molybdenum. Thus, in order to establish the effect of the choice of the initial volume of the platelet on the pressure in the platelet, a platelet formed by the removal of two double $\{110\}$ Ga–As layers was considered and the corresponding pressures calculated using the same procedure as reported before [7, 19]. The pressures obtained for these platelets are indicated by the words “two double $\{110\}$ layers” in Fig. 9.

The plots in Fig. 9 show that the pressures in the platelets at 800°C are below the estimated value for crack propagation. However, considering the fact that all the calculations are subject to approximations, it is significant that the pressures in the uncracked platelets are so close to the theoretical fracture stress. Since the fracture stress decreases with increasing platelet radius, the coalescence of four platelets with radii equal to 17 nm will reduce the value of the fracture stress to $\sim 10^9$ Pa (see Fig. 9 and Table V) which is just above the value of $\sim 6 \times 10^8$ Pa for the pressure in a platelet with radius 17 nm (see Fig. 9 for platelets with two missing double $\{110\}$ layers). It is proposed here that the microsplits were formed when the platelet radius and fracture stress were discontinuously increased and decreased, respectively, by the coalescence of edge-on neighbouring platelets on the same or closed spaced $\{110\}$ planes. Such a process is likely to occur because platelets will attract one another as would dislocation loops of the same configuration. The inference that coalescence of two or more platelets may occur is confirmed by the experimental observation that platelet clusters exist in certain regions of the damaged layer, as shown by the arrows in Fig. 11d below.

The fact that the crack (split) formation occurs at a much lower temperature ($\sim 500^\circ\text{C}$) for the higher-dose ($10^{16} \text{H}^+ \text{cm}^{-2}$) samples than in the case of the lower-dose ($5 \times 10^{15} \text{H}^+ \text{cm}^{-2}$) samples where crack-

ing first occurs at 800°C , can be ascribed to the following facts: firstly, that the maximum platelet diameter in the higher-dose sample is about a factor of 2.5 higher than those in the lower-dose samples; and secondly, that the platelet density is about a factor of 2 higher in the $10^{16} \text{H}^+ \text{cm}^{-2}$ than in the $5 \times 10^{15} \text{H}^+ \text{cm}^{-2}$ dose samples [4]. Thus the higher platelet density together with the larger platelet radii in the higher-dose samples will increase the probability of coalescence of platelets in close proximity, which in turn will result in cracking at lower temperatures compared to the lower-dose samples.

Finally, it was found that annealing for 15 min at 1000°C causes the platelets to disappear from the damaged layer in $5 \times 10^{15} \text{H}^+ \text{cm}^{-2}$ and $10^{16} \text{H}^+ \text{cm}^{-2}$ bombarded samples. Only damage rafts, voids and glissile dislocations generated at the rafts were present in the damaged layer after this heat treatment. It is therefore clear that at 1000°C either all of the platelets contribute to crack formation or the remainder of the platelets are absorbed at the free surfaces of existing microsplits.

The conclusion that the microsplits in these samples occurred as a result of the stresses introduced by the hydrogen gas from the proton bombardment is confirmed by the fact that no microsplits, voids or dislocations were present in high-dose boron-implanted GaAs [25]. Schwuttke [26], using the technique of TEM, observed microsplits in silicon and suggested that they were introduced during the sawing and polishing operations of the silicon wafers. It was also found that microsplits in GaAs [27, 28] and other III–V compounds [29, 30] could be introduced by externally applied stresses. The results of the present study have, however, revealed that stresses produced by gaseous hydrogen from the proton bombardment

TABLE IV Theoretical fracture stress σ at 298 K as a function of crystallographic direction for a platelet ($r = 12.4$ nm) on the (011) planes of GaAs

Property	Crystal plane and directions			
	(011) $[0\bar{1}1]$	(011) $[1\bar{1}1]$	(011) $[3\bar{1}1]$	(011) $[100]$
ν	0.021	0.162	0.366	0.443
σ (10^9 Pa)	2.31	2.34	2.48	2.57

TABLE V Theoretical fracture stress σ at 298 K in the $[0\bar{1}1]$ direction for a platelet on a (011) plane as a function of platelet radius

Radius (nm)	σ (10^9 Pa)
5.6	3.44
8.0	2.87
12.4	2.31
14.4	2.14
16.0	2.03
17.0	1.97
34.0 (2×17.0)	1.39
68.0 (4×17.0)	0.99

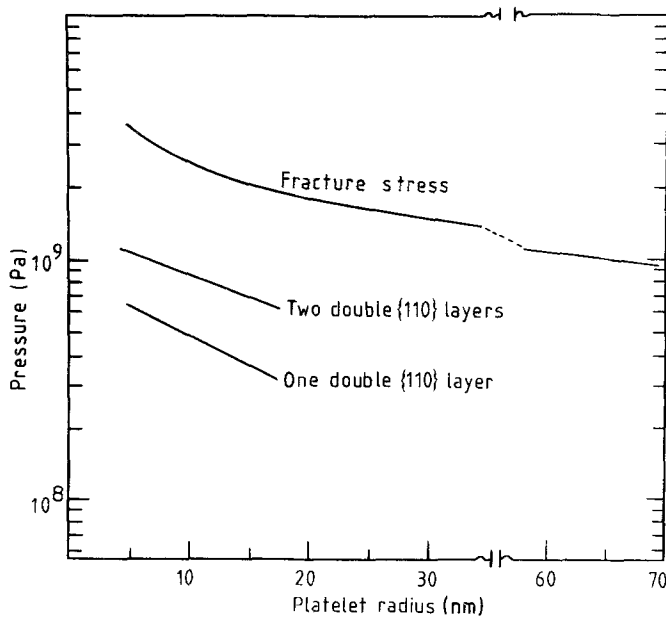


Figure 9 Plots of the theoretical fracture stress and gas pressures as functions of platelet radius. The pressures were calculated at 800°C for platelets consisting of one and two missing double {110} layers.

can also lead to the formation of microsplits in GaAs. This finding is in agreement with the studies done by Takeyama and Takahashi [31, 32] on fracture due to hydrogen embrittlement in iron. These authors suggested that the formation of microcracks by fracture in this metal was caused by the pressure generated by the hydrogen gas which had precipitated in small voids.

3.4. The elongated shape of the damage rafts

An interesting property of the damage rafts was that they were found to lie on the {110} cleavage planes and were elongated along the $\langle 110 \rangle$ directions. This property, which can be explained in terms of the variation in fracture stress with crystallographic direction in the {110} planes, is consistent with the identification of the rafts as microsplits which have closed. The degree of elongation of the rafts was determined by tilting them into planar orientations (see for example the rafts in Fig. 5d and Fig. 11b below) and measuring their dimensions along the perpendicular $\langle 001 \rangle$ and $\langle 110 \rangle$ axes. The ratio of the lengths of their $\langle 001 \rangle$ to $\langle 110 \rangle$ axes was found to lie between 0.32 and 0.36, as can be seen from the results listed in Table VI for three typical examples.

In Fig. 10 a schematic (110) cross-section of a damage raft is shown with the theoretical fracture stress indicated for the various directions in the (110) plane. The fracture stress was calculated for an ellipti-

cal cavity (considered to be a good approximation for a hydrogen platelet) of width 24.8 nm (see Table IV). It is clear from Fig. 10 that the fracture stress is lower in the $[\bar{1}10]$ than in the $[001]$ direction, and therefore it is expected that a crack on a {110} plane will propagate easier along the $\langle \bar{1}10 \rangle$ than the $\langle 001 \rangle$ direction. This property explains the observation that the rafts are always elongated along the $\langle 110 \rangle$ directions with a $\langle 001 \rangle$ to $\langle 110 \rangle$ axis length ratio of ~ 0.3 . In the next section the effect of these microsplits on the surrounding bulk crystal will be discussed. In particular, the capture of vacancies at microsplits, as well as the stress generated at a split, will be investigated.

3.5. Volume swelling and lattice strain

A detailed examination of the damaged layer revealed that the regions around the rafts were denuded of small hydrogen platelets. The rafts apparently act as sinks for the vacancies which would otherwise precipitate in platelets or vacancy loops, if no hydrogen is present. In Fig. 11a a cross-sectional strip of the damaged layer is shown with a raft (A), dislocation (D), voids and platelets (P) indicated. A significant feature of this micrograph, which is also evident in Fig. 2 and in many other observations, is the absence of small platelets near the rafts. The average distance between the rafts and surrounding platelets, obtained

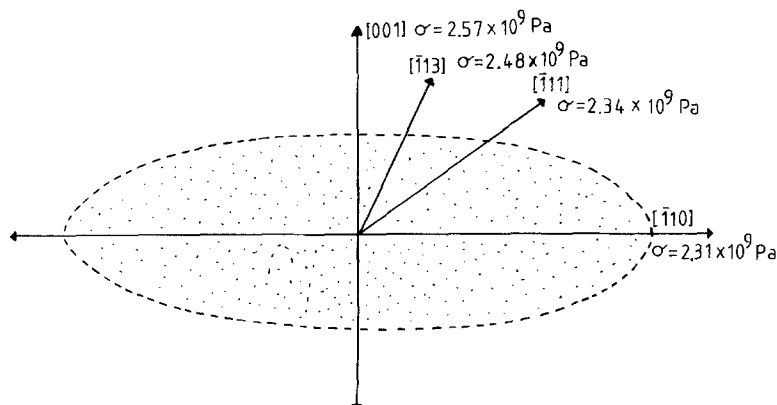


Figure 10 A schematic (110) cross-section of a damage raft constructed according to the dimensions given in Table VI. The fracture stress for a number of directions in the (110) plane is also indicated.

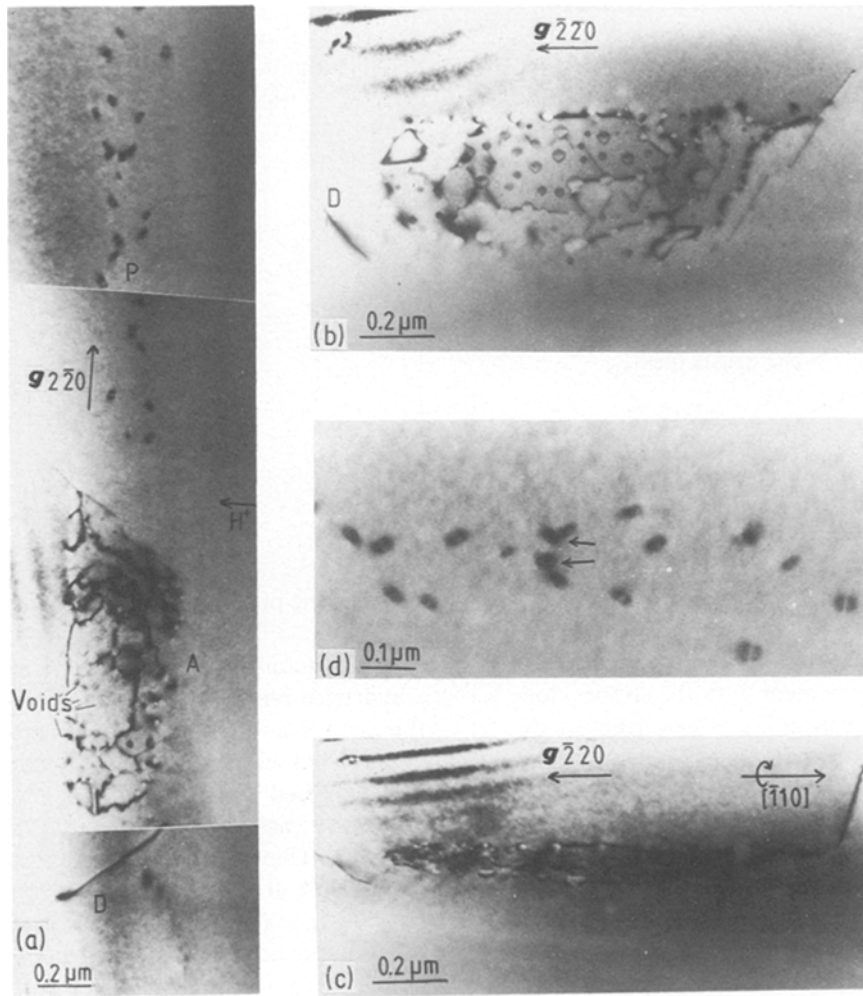


Figure 11 (a) Cross-sectional TEM micrograph showing the defect structure in GaAs implanted with $5 \times 10^{15} \text{ H}^+ \text{ cm}^{-2}$ at 300 keV and annealed at 900° C for 15 min. The damage raft is indicated by (A) and the platelets by (P). The beam direction is close to the $[\bar{1}\bar{1}0]$ direction. In (b) a magnified image of the raft (A) is shown. In (c) the planar nature of the raft is illustrated by tilting the foil about the $[\bar{1}\bar{1}0]$ axis from a $[\bar{1}\bar{1}0]$ beam axis in (b) to a $[\bar{1}\bar{1}2]$ beam axis in (c). In (d) the clustering of some of the platelets in (a) is shown at higher magnification.

from Figs 2 and 11, ranges from 0.4 to $1.2 \mu\text{m}$. In order to establish whether vacancy diffusion can take place over distances of $\sim 1 \mu\text{m}$ during a 15 min anneal at 800° C , a knowledge of the diffusion coefficient for vacancy migration in GaAs is necessary. Because there are not sufficient data available on the diffusion of vacancies in GaAs, it was necessary to look at diffusion studies of vacancies in germanium. The diffusion coefficient for monovacancies in the elemental semiconductors silicon and germanium is given by [33]

$$D_v = \frac{1}{3} d_0^2 \nu \exp\left(\frac{\Delta S_m}{k}\right) \exp\left(\frac{-\Delta H_m}{kT}\right) \quad (3)$$

where $\frac{1}{3}$ is a geometrical factor appropriate to the diamond lattice, d_0 is the interatomic spacing, ν is taken as the lattice vibration frequency, k is Boltzmann's constant and T the temperature. ΔS_m and

ΔH_m are the entropy and enthalpy of vacancy migration, respectively.

The experimentally determined enthalpy for mono-vacancy migration in germanium was found to vary from about 0.2 eV at low temperatures to 1.2 eV at high temperatures [34]. Thus in the present study, where the GaAs samples were annealed at 800° C , we may as a rough estimate use the high-temperature ($\sim 780^\circ \text{ C}$) vacancy annealing data of Hiraki [35] who obtained, for the diffusion of monovacancies, a diffusion coefficient

$$D_v = 2 \exp[-(1.2 \text{ eV})/kT] \text{ cm}^2 \text{ sec}^{-1} \quad (4)$$

The mean distance travelled by the vacancy, $\langle x \rangle$, is given by

$$\langle x \rangle \sim (D_v t)^{1/2} \quad (5)$$

where t is the time of anneal. Setting $T = 1073 \text{ K}$ and $t = 15 \text{ min}$ in Equations 4 and 5, one obtains

$$\langle x \rangle \sim 600 \mu\text{m}$$

In the case of vacancy diffusion in GaAs, only a very rough estimate of the mean distance travelled by a vacancy is possible. According to Lang [36] the entropy factor $\Delta S/k$ for vacancy diffusion in GaAs is estimated to be ~ 8 .

TABLE VI The ratio of the magnitudes of the $\langle 110 \rangle$ to $\langle 001 \rangle$ axes of damage rafts

$\langle 110 \rangle$ axis (μm)	$\langle 001 \rangle$ axis (μm)	$\frac{\langle 001 \rangle}{\langle 110 \rangle}$ axis
1.11	0.40	0.36
1.73	0.56	0.32
1.10	0.40	0.36

Thus taking $d_0 \sim 0.24 \text{ nm}$, $v = 10^{13} \text{ sec}^{-1}$ [37], $\Delta S_m/k = 8$, $\Delta H_m = 1 \text{ eV}$ [38] and $T = 1073 \text{ K}$ in Equation 3, one obtains $D_v = 3 \times 10^{-4} \text{ cm}^2 \text{ sec}^{-1}$. Substituting this value in Equation 5 and setting $t = 15 \text{ min}$, one obtains $\langle x \rangle \sim 0.3 \text{ cm}$ which is about an order of magnitude higher than the value obtained in the case of germanium.

Although this calculation is based on an estimate of the pre-exponential factor, the mean distance travelled by a vacancy in germanium and GaAs during a 15 min anneal at 800°C is at least a few orders of magnitude higher than the average distance of $\sim 1 \mu\text{m}$ between the rafts and surrounding platelets. However, annihilation of the vacancies may occur by vacancy–interstitial recombination (both self-interstitials or hydrogen atoms may annihilate vacancies), and thus the effective diffusion length of the vacancies will be greatly reduced. The observed distance of $\sim 1 \mu\text{m}$ between the rafts and platelets in the present study suggests an effective diffusion length of $\sim 1 \mu\text{m}$ for a vacancy in these proton-bombarded samples. This value is of the same order of magnitude as the diffusion length of $\sim 3.5 \mu\text{m}$ observed for vacancies in proton-bombarded silicon at 900°C [39]. These results thus verify the assumption that the free surfaces of the microsplit act as sinks for the surrounding vacancies and thus create a region denuded of platelets (i.e. hydrogen-filled vacancy loops) around the damage rafts.

In Fig. 11b a magnified image of the raft (A) in Fig. 11a clearly shows the voids and dislocations in the raft plane. Tilting experiments, as already discussed earlier, have indicated that the raft lies in the vicinity of the (110) and (221) planes, while it is elongated in the $[\bar{1}10]$ direction. The fact that this particular raft, in contrast to all the other damage rafts studied, lies close to but not on the (110) plane is not unusual since Allen [29] has indicated that crack propagation in III–V compounds sometimes deviates from the $\{110\}$ cleavage planes. In Fig. 11c the planar nature of the raft is illustrated by tilting the foil through 52° about the $[\bar{1}10]$ axis in the direction indicated.

The formation of voids by the cooperative coalescence of hydrogen atoms and vacancies in the raft will lead to a volume swelling in this region. The magnitude of the volume swelling in the raft was estimated by calculating the void volume density $\Delta V/V$ in the raft. The measurements were based on the assumption that the voids are spherical. The thickness of the raft, as determined by the voids, was measured by tilting it in an edge-on configuration. The volume swelling in the raft shown in Fig. 11b was found to be $\sim 11\%$. Due to the volume swelling in this region, stresses will be introduced in the surrounding material. It is suggested that the dislocations emanating from the rafts (see Figs 13 and 14 below) are introduced to relieve the stress generated by the volume swelling.

The absence of strain contrast around the spherical voids shown in Fig. 11b indicates that the gas pressure P is in equilibrium with the surface tension of the void surface. In this case the pressure is given by [40]

$$P = 2\gamma/r \quad (6)$$

TABLE VII The gas pressure in voids as a function of radius

Radius (nm)	Pressure (10^8 Pa)
6.0	2.8
10.0	1.7
14.0	1.2
20.0	0.9

where r is the void radius and γ the surface energy. Taking $\gamma = 0.86 \text{ J m}^{-2}$ [18], the gas pressure in the voids was calculated as a function of void radius, using Equation 6, and the results are listed in Table VII.

It is interesting to note that the gas pressures in the voids are of the same order of magnitude as the pressures in the platelets (see Fig. 9) of the same radii. However, in the case of the voids the lattice strain around the void has been eliminated by capturing a sufficient number of vacancies so that equilibrium between the pressure and surface tension of the void is attained.

In GaAs bombarded with protons to a dose of $10^{17} \text{ H}^+ \text{ cm}^{-2}$ and annealed at 1000°C the damaged layer contains a high density of voids which lead to a peak volume swelling of 2.5% [4]. In this case, the swelling can expand in a direction perpendicular to the surface and thus eliminate the stress in this direction. Parallel to the surface no relaxation is possible, and thus the large compressive stresses present in the damaged layer will generate tensile stresses in the underlying substrate crystal [41, 42] and also in the surface layer as illustrated in Fig. 12a. The volume swelling in the damaged layer thus subjects the surface layer and underlying substrate crystal to tensile stresses as illustrated in Fig. 12a. In the case of a damage raft, which is held rigid by the surrounding bulk crystal, a volume swelling of $\sim 11\%$ (which is extremely high) in the raft would generate tensile stresses in the surrounding material as schematically illustrated in Fig. 12b. As a consequence of the tensile stresses, shear stresses on the $\{111\}$ slip planes will develop. In the present case, experimental observations indicate that these shear stresses are largely eliminated by glissile dislocations (see Figs 13 and 14) which are generated on the $\{111\}$ slip planes intersecting the rafts on $\{110\}$ planes. It was found that these emitted dislocations are of the $(a/2)\langle 110 \rangle$ type and spread out on the $\{111\}$ planes in a similar manner as usually demonstrated for a Frank–Read source.

In Fig. 13a an edge-on view of a raft (C) lying on the $(1\bar{1}0)$ plane is shown. The rafts were found to act as dislocation sources as reported earlier [5]. By means of tilting experiments it was found that the dislocations (D) generated at the raft (C) spread out on the (111) slip plane and are cut off where they intersect the bottom surface of the foil. In Fig. 13b, the conditions for invisibility for the dislocations generated at the raft (C) in Fig. 13a are shown. Under the two-beam condition with $g = 004$, the only Burgers vectors of the type $(a/2)\langle 110 \rangle$ which would be invisible are those with $\mathbf{b} = \pm (a/2)[1\bar{1}0]$. This Burgers vector is characteristic of the type of glissile dislocation usually associated with the GaAs structure [43].

In Figs 13c and d wider projected images of the raft

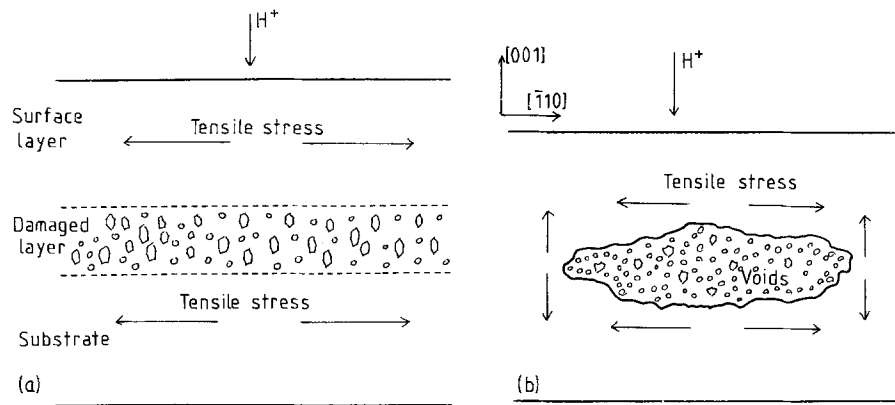


Figure 12 Schematic representation of the stresses generated by the swelling in the damaged layer of (a) a high-dose proton-bombarded sample and (b) in the case of a damage raft.

shown in Fig. 13a are obtained by tilting through 27° about the $[001]$ axis in the directions indicated. It can be seen in Fig. 13c that the raft consists of a planar array of voids lying on the $(\bar{1}10)$ plane. Another example of the voids present in a raft is shown in Fig. 13e. The generation of the two glissile disloca-

tions (D) at the intersection of the (111) plane with the $(\bar{1}10)$ plane of the raft is also clearly illustrated in Figs 13c and d. The cut-off dislocations (D) generated at the raft in Fig. 13a clearly represents the leading section of a Frank-Read source [44] while the cut-off dislocations generated at the raft (E) in Fig. 14a

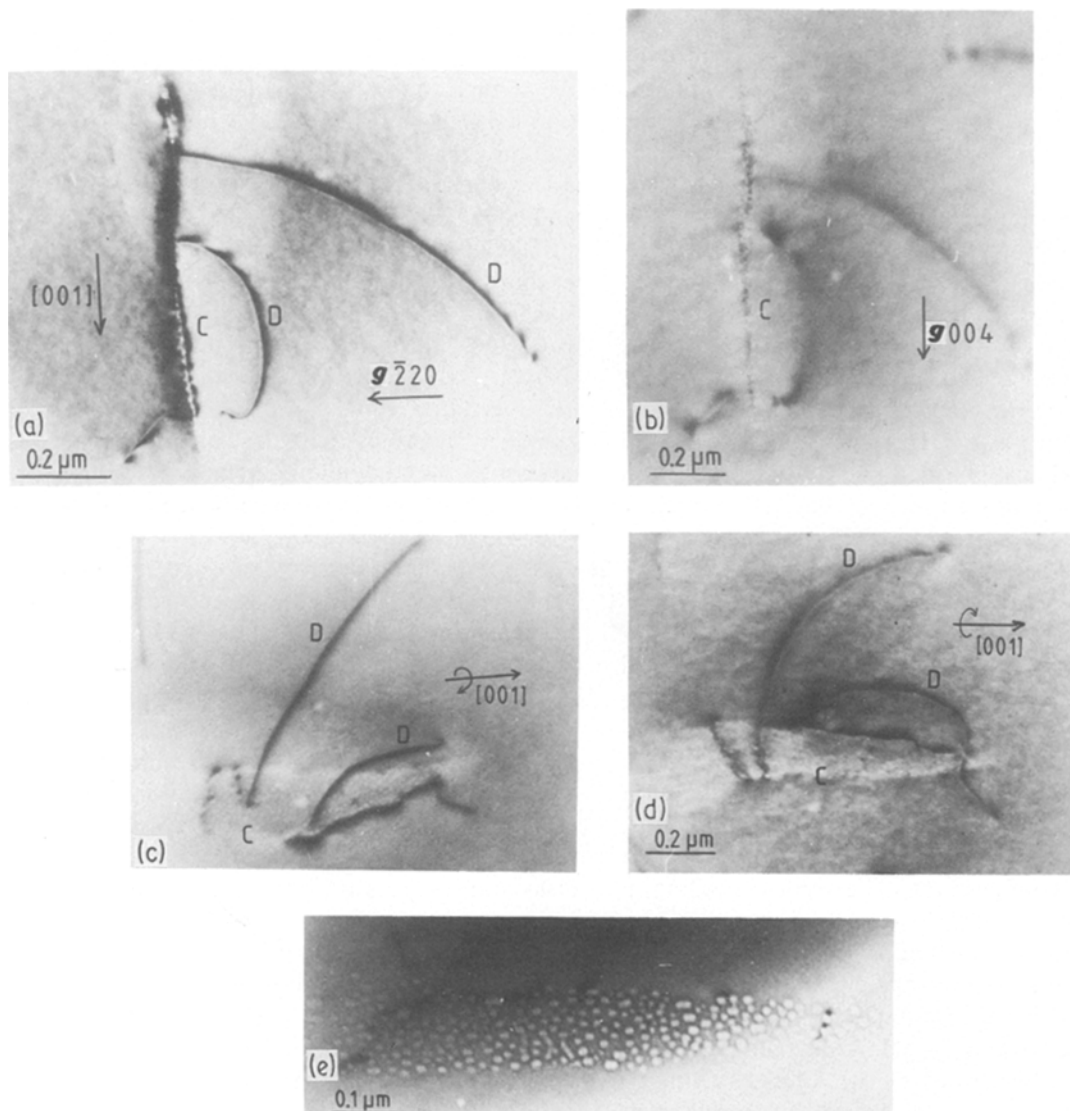


Figure 13 (a) A damage raft (C) on a $(\bar{1}10)$ plane which acts as a dislocation source in GaAs implanted with $10^{16} \text{H}^+ \text{cm}^{-2}$ at 300 keV and annealed at 800°C for 15 min. The dislocations (D) spread out on the (111) slip plane. In (b) the condition for invisibility of the dislocations (D) generated at the raft is shown. The beam axis in (a) and (b) is close to the $[\bar{1}10]$ direction. In (c) and (d), wider projected images of the raft (C) are obtained after tilting through 27° about the $[001]$ axis in the directions indicated. (e) Micrograph showing the voids in a raft on a $(10\bar{1})$ plane (dose $5 \times 10^{15} \text{H}^+ \text{cm}^{-2}$, annealed at 900°C for 15 min).

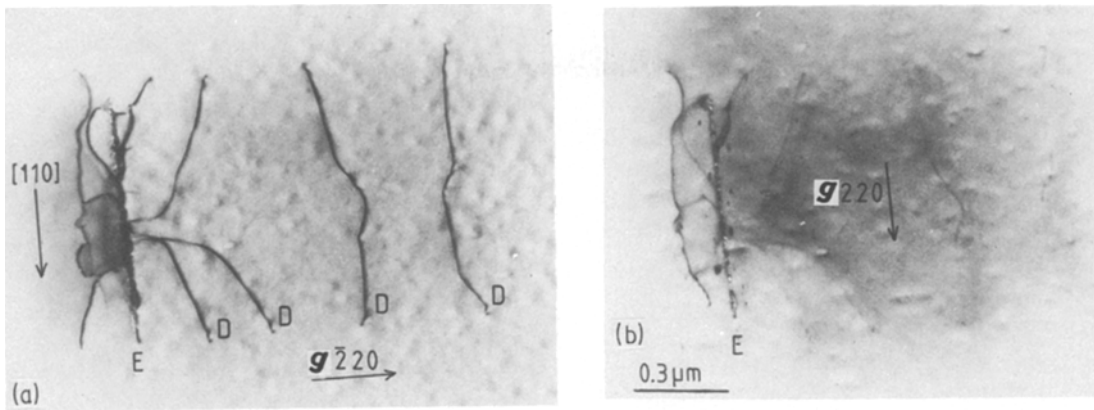


Figure 14 An edge-on view of a raft on the $(\bar{1}10)$ plane in a planar thinned GaAs sample implanted with $10^{16} \text{H}^+ \text{cm}^{-2}$ at 300 keV and annealed at 500°C for 15 min. The dislocations (D) generated at the raft spread out on the $(\bar{1}\bar{1}1)$ slip plane. In (b) the conditions for invisibility of most of the dislocations generated at the raft (E) are shown. The beam axis is close to the $[00\bar{1}]$ direction.

represents the closure sections of the loops generated by the source.

In Fig. 14a an edge-on view of a damage raft (E) in a planar thinned sample is shown. The dislocations (D), generated at the raft (E) on the $(\bar{1}10)$ plane, are seen to spread out on a slip plane that can be identified as the $(\bar{1}\bar{1}1)$ by sample tilting and are cut off where they intersect the top and bottom surfaces of the foil. In Fig. 14b the conditions for invisibility of most of the dislocations generated near the raft (E) in Fig. 14a are shown. Under the two-beam condition with $g = 220$, the only Burgers vectors of the type $(a/2)\langle 110 \rangle$ which would be invisible are those with $b \pm (a/2)[\bar{1}10]$. This Burgers vector again is common to the GaAs structure [45]. It is interesting to notice that the glissile dislocation furthest from the raft in Fig. 14 has glided over a distance of about $1 \mu\text{m}$.

It was suggested in the beginning of this section that these glissile dislocations are introduced at the rafts to relieve the stresses generated between the raft and surrounding bulk crystal as a result of the volume swelling in the raft. An estimation of the magnitude of the stresses involved in the dislocation generation can be obtained by calculating the shear stress τ_0 required to bend one of these glissile dislocations to a radius R .

This stress is given [44] by

$$\tau_0 = \frac{0.5\mu b}{R} \quad (7)$$

where μ is the shear modulus, b the Burgers vector and R the radius of curvature.

For the half-loops with $b = (a/2)\langle 110 \rangle$ shown in Figs 5a and 13a the radii of curvature were measured to be 0.43 and $0.33 \mu\text{m}$, respectively. Substituting these values in Equation 7 and taking $\mu = 4.9 \times 10^{10} \text{Nm}^{-2}$ [19] one obtains for the shear stresses values of $\sim 2 \times 10^7$ and $3 \times 10^7 \text{Pa}$ for the half-loops in Figs 5a and 13a, respectively. However, it is clear from Equation 7, that the shear stress required to expand the half-loops will decrease with increasing R (or distance from the raft), and therefore the stress required to nucleate these dislocations will be higher than the values to propagate them or keep them in configurational equilibrium. The peak compressive stress (as a result of volume swelling [42]) in the implanted region of a proton-bombarded ($5 \times 10^{15} \text{H}^+ \text{cm}^{-2}$ at 140 keV) fused silica sample was measured by EerNisse [46] to be of the order of 10^8Pa . This result thus indicates that larger shear stresses will develop on $\{111\}$ planes in the bulk material surrounding the

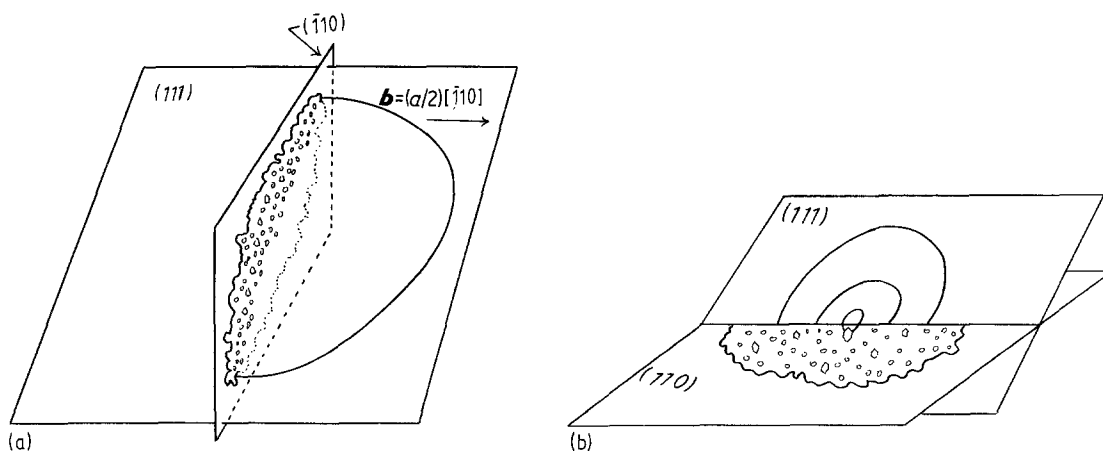


Figure 15 (a) Schematic representation of the generation of a glissile dislocation on a (111) plane at the intersection of a damage raft on a $(\bar{1}10)$ plane (see for example the raft in Fig. 13). In (b) the nucleation of a dislocation at the point of a void which acts as a stress concentrator is shown. The dislocations then spread out on the (111) plane.

raft. It is suggested that the sharp points of faceted voids or very small voids, present in the rafts, may act as stress concentrators and provide surface sources for the generation of glissile dislocations which will then spread out on the $\{111\}$ slip planes intersecting the $\{110\}$ planes of the rafts. This process is schematically illustrated in Figs 15a and b. Other examples of the generation of glissile dislocations at damage rafts are given elsewhere [4].

4. Summary and conclusion

The precipitated damage in low-dose (10^{15} and $5 \times 10^{15} \text{ H}^+ \text{ cm}^{-2}$) proton-bombarded GaAs annealed at temperatures of 500°C and above was found to consist of hydrogen platelets (i.e. hydrogen-filled vacancy loops) on the $\{110\}$ cleavage planes of GaAs. It is suggested that these platelets were formed by the cooperative coalescence of hydrogen atoms and vacancies during the 15 min annealing process. However, in the $5 \times 10^{15} \text{ H}^+ \text{ cm}^{-2}$ samples annealed at 800°C and above, or the $10^{16} \text{ H}^+ \text{ cm}^{-2}$ samples annealed at 500°C and above, the damage precipitation was heterogeneous, consisting not only of platelets but also containing damage rafts (i.e. three-dimensional dislocation-void clusters).

The damage rafts were found to consist of planar arrays of voids on the $\{110\}$ planes and were elongated along the $\langle 110 \rangle$ directions. It is proposed that damage rafts originate at microsplits on the $\{110\}$ cleavage planes of GaAs, following the cracking open of small hydrogen-filled platelets when the internal gas pressure exceeds that which is necessary for crack propagation. It was shown that the edge-on coalescence of a few hydrogen platelets will lead to a situation where the internal gas pressure in the platelet cluster will approach the theoretical fracture stress of GaAs along the $\{110\}$ planes. The presence of voids in the raft plane is consistent with the model of a microsplit where the free surfaces of the split act as a sink for surrounding vacancies.

The elongation of the rafts on (110) planes was characterized by a $[001]$ to $[\bar{1}\bar{1}0]$ axis ratio of ~ 0.3 . This result was explained in terms of the lower fracture stress in the $[\bar{1}\bar{1}0]$ than in the $[001]$ direction which is a result of the elastic anisotropy of GaAs. The presence of jagged line dislocations in the raft plane indicates that the microsplit has closed but healed imperfectly. It was shown that these dislocations, which were probably introduced due to the mismatch of the two surfaces, could have Burgers vectors of the type $\pm(a/2)[\bar{1}10]$, $\pm a[001]$ and $\pm(a/2)[\bar{1}12]$ lying in the (110) plane of the split.

The critical temperature and proton dose for microsplit formation in GaAs were determined to be $5 \times 10^{15} \text{ H}^+ \text{ cm}^{-2}$ for samples annealed at 800°C , or $10^{16} \text{ H}^+ \text{ cm}^{-2}$ for samples annealed at 500°C . The annealing time in both cases was 15 min.

From a consideration of the distances between damage rafts and hydrogen platelets, an average diffusion length of $\sim 1 \mu\text{m}$ was estimated for vacancies in proton-bombarded GaAs at $\sim 900^\circ\text{C}$.

The volume swelling in a typical damage raft was calculated to be $\sim 11\%$.

Glissile dislocations of the type $(a/2)\langle 110 \rangle$ are generated on the $\{111\}$ slip planes, intersecting the rafts on $\{110\}$ planes, in a similar manner to that usually demonstrated for a Frank-Read source. It is suggested that the shear stresses which develop as a consequence of the volume swelling in the raft are responsible for the generation of these dislocations. The glissile dislocations generated at the rafts were found to glide over distances of about $1 \mu\text{m}$ during the 15 min anneal at temperatures in the range 500 to 800°C .

The glissile dislocations observed in the present study are similar to the straight-line $\langle 110 \rangle$ dark-line defects observed in degraded $\text{Ga}_{1-x}\text{Al}_x\text{As}$ laser devices [47, 48]. It is thus concluded that the radiation damage together with the hydrogen gas in proton-bombarded GaAs are responsible for the formation of microsplits, which if present in a double heterostructure laser [49] will generate glissile dislocations which may spread into the stripe (active) region and lead to the degradation of the device. A discussion of the similarity between the damage rafts and dislocations generated at the rafts and the dark-line defects found in degraded $\text{Ga}_{1-x}\text{Al}_x\text{As}$ laser devices will be published elsewhere.

A recent calculation of the gas pressures in hydrogen platelets, using a more accurate model than before [7], revealed that the room-temperature pressure in the platelets is of the order of 10^9 Pa [19].

Acknowledgements

The authors wish to thank the Council for Scientific and Industrial Research of South Africa for financial assistance and the Electronic Engineering Department at the Rand Afrikaans University for doing the proton implantation.

References

1. E. GARMIRE, H. STOLL, A. YARIV and R. G. HUNSPERGER, *Appl. Phys. Lett.* **21** (1972) 87.
2. J. C. DYMENT, J. C. NORTH and L. A. D'ASARO, *J. Appl. Phys.* **44** (1973) 207.
3. H. C. SNYMAN and J. H. NEETHLING, *Rad. Effects* **60** (1982) 147.
4. *Idem, ibid.* **69** (1983) 199.
5. J. H. NEETHLING and H. C. SNYMAN, *Rad. Effects. Lett.* **76** (1983) 163.
6. *Idem, J. Appl. Phys.* **60** (1986) 941.
7. J. H. NEETHLING, H. C. SNYMAN and C. A. B. BALL, in Proceedings of the 13th International Conference on Defects in Semiconductors, August 1984, edited by L. C. Kimerling and J. M. Parsey (Metallurgical Society, Coronado, California, 1984) p. 427.
8. J. F. GIBBONS, W. S. JOHNSON and S. W. MYLROIE, "Projected Range Statistics", 2nd Edn (Dowden, Hutchinson and Ross, Stroudsburg, Pennsylvania, 1975) p. 29.
9. C. HILSUM and A. C. ROSE-INNES, in "Semiconducting III-V Compounds" (Pergamon, Oxford, 1961) p. 86.
10. J. A. Van VECHTEN, *J. Physica B & C* **116** (1983) 575.
11. J. R. LLOYD and S. NAKAHARA, *J. Electrochem. Soc.* **125** (1978) 2037.
12. J. W. EDINGTON, in "Practical Electron Microscopy in Materials Science", Vol. 3 (MacMillan, London, 1975) p. 66.
13. T. J. MAGEE, *Phys. Status Solidi (a)* **26** (1974) 425.
14. J. W. ALLEN, *Phil. Mag.* **4** (1959) 1046.
15. P. W. HUTCHINSON and P. S. DOBSON, *ibid.* **32** (1975) 745.

16. *Idem*, *Phil. Mag. A* **41** (1980) 601.
17. J. J. COMER, *Rad. Effects* **36** (1978) 57.
18. C. MESSMER and J. C. BILELLO, *J. Appl. Phys.* **52** (1981) 4623.
19. J. H. NEETHLING, H. C. SNYMAN and C. A. B. BALL, *ibid.* **59** (1988) 704.
20. S. P. ARDREN, C. A. B. BALL, J. H. NEETHLING and H. C. SNYMAN, *ibid.* **60** (1986) 965.
21. W. A. BRANTLEY, *ibid.* **44** (1973) 534.
22. R. I. COTTAM and G. A. SAUNDERS, *J. Phys. C: Solid State Phys.* **6** (1973) 2105.
23. Yu. A. BURENKOV, Yu. M. BURDUKOV, S. Yu. DAVYKOV and S. P. NIKANOROV, *Sov. Phys. Solid State* **15** (1973) 1175.
24. J. H. EVANS, A. Van VEEN and L. M. CASPERS, *Scripta Metall.* **17** (1983) 549.
25. H. C. SNYMAN, J. H. NEETHLING and C. A. B. BALL, in Proceedings of the 18th International Conference on Solid State Devices and Materials, 20–22 August, 1986, Tokyo (Japan Society for Applied Physics, Tokyo, 1986) p. 745.
26. G. H. SCHWUTTKE, in Proceedings of the Symposium on Material Science Aspects of Thin Film Systems for Solar Energy Conversion, 20–22 May, 1974, Tucson, Arizona, edited by B. O. Seraphin (National Science Foundation, Tucson, 1974) p. 49.
27. R. U. KHOKHAR and D. HANEMAN, *Solid State Electron.* **13** (1970) 439.
28. *Idem*, *ibid.* **15** (1972) 948.
29. J. W. ALLEN, *Phil. Mag.* **4** (1959) 1046.
30. J. J. COMER, *J. Appl. Phys.* **50** (1979) 6003.
31. T. TAKEYAMA and H. TAKAHASHI, in Proceedings of Conference on Hydrogen in Metals, 26–29 November, 1979, Minakami, Gunma Pref., Japan (Japan Institute of Metals, Aoba Aramaki, Sendai 980, Japan, 1980) p. 409.
32. *Idem*, in Proceedings of US–Japan Seminar on the Mechanical Properties of BCC Metals, 23–27 March, 1981, Honolulu, Hawaii, edited by M. Meshii (Metallurgical Society of AIME, Honolulu, Hawaii, 1981) p. 135.
33. J. A. Van VECHTEN, *Phys. Rev. B* **10** (1974) 1482.
34. *Idem*, *ibid.* **12** (1975) 1247.
35. A. HIRAKI, *J. Phys. Soc. Jpn* **21** (1966) 34.
36. D. V. LANG, in “Radiation Effects in Semiconductors 1976”, Institute of Physics Conference Series No. 31, 6–9 September 1976, Dubrovnik (Institute of Physics, Bristol, UK, 1977) p. 70.
37. P. W. HUTCHINSON and P. S. DOBSON, *J. Mater. Sci.* **10** (1975) 1636.
38. H. R. POTTS and G. L. PEARSON, *J. Appl. Phys.* **37** (1966) 2098.
39. B. J. MASTERS, “Defects and Radiation Effects in Semiconductors 1978”, Institute of Physics Conference Series No. 46, 11–14 September, 1978, Nice (Institute of Physics, Bristol, UK, 1979) p. 545.
40. J. H. EVANS, *J. Nucl. Mater.* **68** (1977) 129.
41. K. SESHAN and E. P. EERNISSE, *Appl. Phys. Lett.* **33** (1978) 21.
42. J. ROTH, in “Applications of Ion Beams to Materials 1975”, Institute of Physics Conference Series No. 28 (1976) p. 280.
43. D. LAISTER and G. M. JENKINS, *J. Mater. Sci.* **8** (1973) 1218.
44. A. H. COTTRELL, “Dislocations and Plastic Flow in Crystals” (Clarendon, Oxford, 1953) p. 84.
45. D. J. STIRLAND and B. W. STRAUGHAN, *Thin Solid Films* **31** (1976) 139.
46. E. P. EERNISSE, in “Ion Implantation in Semiconductor and other Materials”, edited by B. L. Crowder (Plenum, New York, 1973) p. 531.
47. K. ENDO, S. MATSUMOTO, H. KAWANO and I. SAKUMA, *Appl. Phys. Lett.* **40** (1982) 921.
48. O. UEDA, S. ISOZUMI, S. YAMAKOSHI and T. KOTANI, *J. Appl. Phys.* **50** (1979) 765.
49. P. PETROFF and R. L. HARTMAN, *Appl. Phys. Lett.* **23** (1973) 469.

*Received 25 March
and accepted 8 June 1987*